

Title:

FDTD Analysis of 100%-Efficient Polarization-Independent
Liquid Crystal Polarization Gratings

Authors:

Chulwoo Oh, Ravi Komanduri, and Michael J. Escuti

Affiliation:

North Carolina State University, Dept Electrical & Computer Engineering, Raleigh, NC (USA)

Presented At:

SPIE Optics & Photonics Conference, San Diego, CA (August 13-17, 2006)

Citation:

C. Oh, R. Komanduri, and M.J. Escuti, "FDTD Analysis of 100%-Efficient Polarization-Independent Liquid Crystal Polarization Gratings", *Proceedings of SPIE*, vol. **6332**, no. 633212 (2006).

Copyright 2006 Society of Photo-Optical Instrumentation Engineers.

This paper was published in Proceedings of SPIE Vol. 6332 and is made available as an electronic reprint with permission of SPIE. One print or electronic copy may be made for personal use only. Systematic or multiple reproduction, distribution to multiple locations via electronic or other means, duplication of any material in this paper for a fee or for commercial purposes, or modification of the content of this paper are prohibited.

FDTD Analysis of 100%-Efficient Polarization-Independent Liquid Crystal Polarization Gratings

Chulwoo Oh, Ravi Komanduri and Michael J. Escuti

Dept. of Electrical and Computer Engineering, North Carolina State Univ., Raleigh, NC, USA

ABSTRACT

We report a numerical analysis of the liquid crystal polarization grating (LCPG) as an electro-optically controlled, polarization independent light modulator. The 2D finite-difference time-domain (FDTD) modeling for periodic anisotropic structures has been developed as a numerical tool to study optical properties of anisotropic gratings. Both normal and oblique incidence cases are successfully implemented for wide-band analysis. Nematic director profiles of the LCPG are obtained from elastic free-energy calculations using a commercial software tool, called LC3D. A study of the essential diffraction characteristics of the LCPG is presented, which manifests pixel-level light modulation with a nearly 100% efficiency on unpolarized light. The effect of an off-axis input and the grating regime on the LCPG diffraction is investigated. Finally, we present a study of the electro-optical response of the LCPG when an electric field applied for both static and dynamic cases. The FDTD results show that a highly efficient, polarization-independent light modulation with capability of an electrical switching/tuning is possible by the LCPG.

Keywords: polarization grating, FDTD, liquid crystal, light modulator

1. INTRODUCTION

Researchers have searched for compact, highly efficient, and low-voltage-driving LC devices as a light modulator/grating for various applications including projection displays, beam steering, optical storage, tunable spectral filters, and diffractive optics. Bos and coworkers proposed several liquid crystal (LC) binary gratings, potentially highly efficient and polarization-independent.¹⁻⁴ However, these LC gratings were plagued by disclination lines and relatively large grating periods due to the discrete nature of binary gratings.

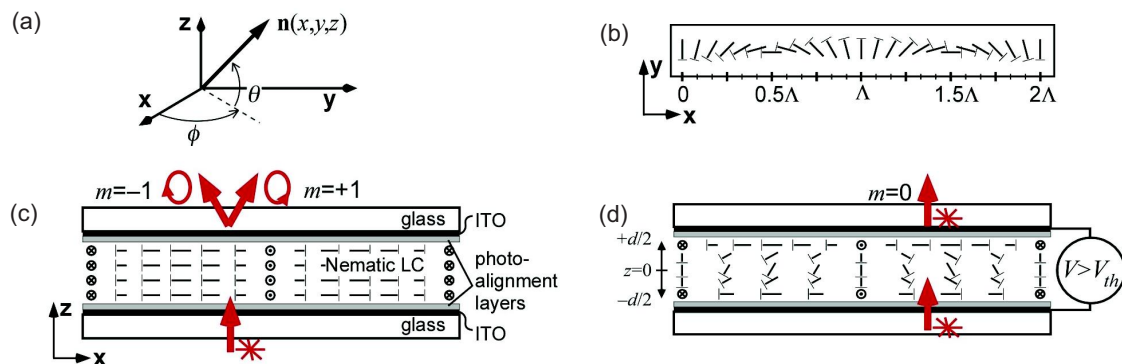


Figure 1. The liquid crystal polarization grating (LCPG): (a) orientation of nematic director, (b) top-view and (c) side-view of the well-aligned diffracting state ($V_A < V_{th}$ and $d < d_C$), and (d) side-view when thresholds are exceeded ($V_A > V_{th}$ or $d > d_C$).

The polarization grating (PG) is a polarization-selective optical element composed of a periodically varying anisotropy as shown in Fig. 1(b). Since the first report of PGs appeared in Soviet journals,⁵ the diffraction

Further author information: (Send correspondence to M.J.E., e-mail: mjescuti@ncsu.edu)

properties of PG have been studied through theoretical and experimental works by many research groups.⁶⁻⁹ PGs operate by periodically modulating the state of polarization of light passing through them. The most distinct feature of PGs from conventional gratings is its Bragg property, $\sim 100\%$ diffraction efficiency into the first order(s), with a thin-grating structure regardless of input polarization.

The primary means for creating PGs is using polarization holography with anisotropic organic recording materials (e.g. azo-containing polymers or azo-dyed glasses).^{6,10,11} An effective fabrication technique for creating PGs employing photo-alignment techniques was proposed.^{12,13} However, PGs of the initial experiments suffered from defects, degrading their optical properties. Recently, we have succeeded to experimentally realize high-quality liquid crystal PGs (LCPGs) by a careful choice of LC and photo-alignment materials.¹⁴

The LCPG owes its unique optical properties to a spatially-varying uniaxial birefringence in the grating plane that can be embodied in a nematic director described as $\mathbf{n}(x) = [\sin(\pi x/\Lambda), \cos(\pi x/\Lambda), 0]$, where Λ is half of the nematic period (P). Simple analytic expressions for diffraction efficiencies can be obtained using the 2×2 Jones matrix method:¹⁴

$$\eta_0 = \cos^2 \left(\frac{\pi \Delta n d}{\lambda} \right) \quad (1)$$

$$\eta_{\pm 1} = \frac{1 \mp S'_3}{2} \sin^2 \left(\frac{\pi \Delta n d}{\lambda} \right) \quad (2)$$

where η_m is the diffraction efficiency of the m^{th} order, Δn is the birefringence of liquid crystals, d is the cell gap, λ is the wavelength of incident light, and $S'_3 = S_3/S_0$ is the normalized Stokes parameter corresponding to the ellipticity angle of input polarization. Note that the paraxial approximation and a thin grating with the infinite width at normal incidence are assumed to derive the analytical solutions.

From Eq. 1 and 2, the unique diffraction characteristics of the LCPG can be summarized:

1. the 0^{th} order is polarization independent;
2. the first orders show 100% diffraction efficiency when $\Delta n d = \lambda/2$;
3. the first orders have polarization selectivity, but the sum is constant over arbitrary input polarization.

These essential optical properties of the LCPG were confirmed by a numerical analysis using the finite-difference time-domain (FDTD) method.¹⁵ In addition, the elastic continuum analysis of the LCPG in Ref. 15,16 predicts that the LC configuration in the grating will be deformed when the thickness (d) is larger than the critical thickness d_C or when an applied voltage (V_A) exceeds the threshold value V_{th} .

An electro-optic switching or tuning occurs in the LCPG as an applied field reorients the nematic director out of plane, decreasing the effective retardation. The reorientation of liquid crystals leads in a coupling of energy between the 0^{th} order and the $\pm 1^{\text{st}}$ orders. Fig. 1(d) shows an example of electrical switching of the LCPG when $V_A > V_{th}$.

In this paper, computer simulations are used to study the optical properties of the LCPG. We combined the modified FDTD method for periodic anisotropic media with a liquid crystal director modeling tool called LC3D.¹⁷ LC director configurations from LC3D results are used for the FDTD optical simulations. First, we present the diffraction spectra and polarization selectivity of the LCPG. Then, the diffraction properties for oblique incidence and the paraxial limit of the LCPG are studied. Finally, we test the electro-optical response of the LCPG for both static and dynamic case.

2. NUMERICAL METHOD DESCRIPTION

2.1. Liquid crystal director calculations

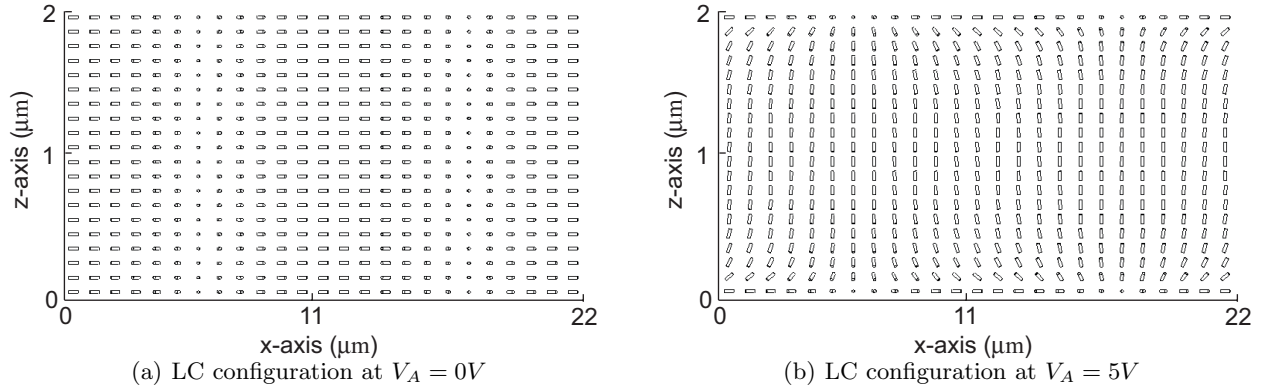
Material parameters of liquid crystal MLC-6080¹⁸ (Merck) are used for the LC configuration calculations. LC material parameters are given in Table 1. A strong anchoring condition is assumed for both top and bottom substrates.

Table 1. Material parameters of MLC-6080

Parameter	Numerical value
Elastic constants (pN)	$k_{11} = 14.4, k_{22} = 7.1, k_{33} = 19.1$
Relative dielectric constants	$\varepsilon_{\perp} = 3.9, \varepsilon_{\parallel} = 11.1$
Refractive indices	$n_{\perp} = 1.5, n_{\parallel} = 1.7$

The grating thickness is $d = 2\mu m$ and the optical pitch is $\Lambda = 11\mu m$, which is a half of the nematic period $P = 22\mu m$. From Eq. 2, the maximum diffraction into the first orders can occur when the grating parameters satisfy the $\lambda/2$ retardation condition ($\Delta nd = \lambda/2$). The LCPG can be tuned by applying electric fields across the cell to get the maximum diffraction efficiency at a certain wavelength.

We calculated the equilibrium LC configurations to minimize the total elastic energy with varying an applied voltage across the cell. To study the dynamics during transitions of “ON” and “OFF” switching, we also calculated the dynamic LC director response during switching. The pre-tilt angle is assumed 0 for the static cases while 1° for the dynamic cases because the LC3D results become unstable without a small pre-tilt. Fig. 2(a) and 2(b) illustrate the calculated LC configurations corresponding to applied voltage of 0V and 5V, respectively. The numerical calculations were carried out with a $440nm \times 100nm$ grid-spacing, and then we interpolated the results for a finer grid of $10nm \times 10nm$, which is suitable for the FDTD optical simulations.

**Figure 2.** Nematic director orientation profiles for the LCPG at different applied voltages: (a) $V_A = 0V$; (b) $V_A = 5V$.

2.2. Finite-Difference Time-Domain method

We examine the optical properties of the LCPG with various grating parameters. To this end, we apply the 2-D finite-difference time-domain (FDTD) method for periodic anisotropic media. The FDTD method is a numerical technique to directly solve for Maxwell’s time-dependent curl equations based on the Yee algorithm.¹⁹

For source-free anisotropic media, Maxwell’s equations can be written as

$$\frac{\partial \mathbf{E}(r)}{\partial t} = \varepsilon_0 \tilde{\varepsilon}^{-1}(r) \cdot [\nabla \times \mathbf{H}(r)] \quad (3)$$

$$\frac{\partial \mathbf{H}(r)}{\partial t} = -\mu_0^{-1} \cdot [\nabla \times \mathbf{E}(r)] \quad (4)$$

where $\tilde{\varepsilon}^{-1}(r)$ is the inverse of the optical dielectric tensor that describes the uniaxial birefringence of a nematic director at a position r . The dielectric tensor $\tilde{\varepsilon}$ can be determined by two angles, the azimuth angle (ϕ) and the

tilt angle (θ) of a nematic director:

$$\tilde{\epsilon} = \begin{bmatrix} \sin \phi & \cos \theta \cos \phi & \sin \theta \cos \phi \\ -\cos \phi & \cos \theta \sin \phi & \sin \theta \sin \phi \\ 0 & -\sin \theta & \cos \theta \end{bmatrix} \begin{bmatrix} n_{\parallel}^2 & 0 & 0 \\ 0 & n_{\perp}^2 & 0 \\ 0 & 0 & n_{\perp}^2 \end{bmatrix} \begin{bmatrix} \sin \phi & -\cos \phi & 0 \\ \cos \theta \cos \phi & \cos \theta \sin \phi & -\sin \theta \\ \sin \theta \cos \phi & \sin \theta \sin \phi & \cos \theta \end{bmatrix}. \quad (5)$$

where n_{\perp} and n_{\parallel} are the ordinary (perpendicular) and extraordinary (parallel) refractive indices, respectively. The information of two orientation angles (ϕ and θ) can be extracted from the results of LC3D calculations for the LC configuration of the LCPG.

For periodic media, the simulation space can be reduced into a unit structure by applying periodic boundary conditions (PBCs). The FDTD implementation of PBCs is straightforward in the case of normal incidence. However, at oblique incidence, phase variation across the Yee grid cells leads in a time-advance or -retardation, which cannot be directly solved in the time-domain. This difficulty can be circumvented using a new set of field variables: $\mathbf{P} = \mathbf{E} \exp(jk_x x)$ and $\mathbf{Q} = 120\pi \mathbf{H} \exp(jk_x x)$. Substituting P and Q fields variables into Eq. 6 and 7, the modified Maxwell's equations in the frequency domain now become:

$$\frac{j\omega}{c} \mathbf{P}(r) = \tilde{\epsilon}^{-1}(r) \cdot [\nabla \times \mathbf{Q}(r)] \quad (6)$$

$$\frac{j\omega}{c} \mathbf{Q}(r) = -\nabla \times \mathbf{P}(r) \quad (7)$$

where c is the speed of light in the vacuum, ω is the angular frequency defined as $2\pi f$.

The FDTD solution for these new equations may involve a considerable complexity. An efficient FDTD implementation method is the split-field update technique, proposed by A. Roden and his coworkers.²⁰ However, the previous work was limited to material properties with diagonal tensors. We expanded the split-field FDTD method for more general anisotropic media having non-diagonal tensors. The complete FDTD formulations can be found in Ref. 21.

Two remaining boundaries must be treated by a proper boundary condition to avoid non-physical reflections. The computational space truncation can be done by placing artificially absorbing media with nearly zero reflection. We construct absorbing boundaries using the Uniaxial Perfectly Matched Layer (UPML) technique²² because the UPML shows the best performance as a absorbing boundary condition and it can be also easily implemented in the split-field FDTD method.

Fig. 3 illustrates a 2-D geometry for FDTD simulations. The LCPG can be defined in the FDTD domain by mapping the calculated director configuration into the dielectric tensor. Graded-index antireflection layers²³

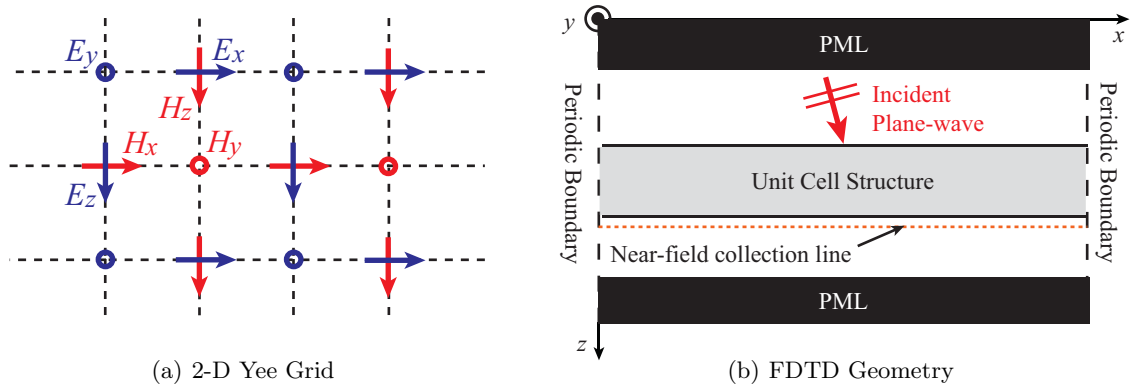


Figure 3. Schematic view of (a) bi-dimensional Yee grid and (b) 2-D FDTD computational space.

are placed at the face and back of the LCPG to minimize reflections at the air-LCPG interfaces due to index mismatch. We use a standard Gaussian pulse as an input signal for wide-band analysis.

The far-field information for the Floquet mode m can be obtained by collecting the near-field results right behind the LCPG and transforming them as follows:

$$E_{TE, far}^m(t) = \frac{1}{\Lambda} \int_0^\Lambda [P_{x, near}(t, x) \cos \theta_m - P_{z, near}(t, x) \sin \theta_m] \exp\left(j \frac{2\pi m}{\Lambda} x\right) dx \quad (8)$$

$$E_{TM, far}^m(t) = \frac{1}{\Lambda} \int_0^\Lambda P_{y, near}(t, x) \exp\left(j \frac{2\pi m}{\Lambda} x\right) dx \quad (9)$$

where the subscripts “ TE ” and “ TM ” represent the TE - and TM -components of the far-field for the m -th order of diffraction. The LCPG follows the normal grating equation, $\theta_m = \sin^{-1}(m\lambda/\Lambda)$. Then, the DFT is applied at every time-step to extract the frequency information.

The maximum Yee grid spacing (Δu) is $1/40^{th}$ of the center wavelength (λ_0) and the time-resolution (Δt) is $\Delta u/3c$. The typical simulation parameters are summarized in Table 2.

Table 2. FDTD Simulation Parameters

Parameter	Normalized value	Sampled value
Spacial resolution (Δu)	$\lambda_0/40$	20nm
Temporal resolution (Δt)	$\Delta x/3c$	0.022fs
Gaussian pulse width (T)	$50\Delta t$	0.11fs
PML thickness	$40\Delta u$	800nm

3. NUMERICAL ANALYSIS OF LC POLARIZATION GRATINGS

The most unique feature of the LCPG is its 100% diffraction (a Bragg property) with a thin grating structure. Fig. 4(a) and 4(b) shows the near-field images of the electric field for linear and circular input polarization when $\Delta nd = \lambda/2$ and $\Lambda = 40\lambda$. The calculated diffraction efficiencies are illustrated in Fig. 5(a) as a function of the normalized retardation ($\Delta nd/\lambda$). Only three diffraction orders (the 0^{th} and $\pm 1^{st}$) appear in the LCPG diffraction. The maximum diffraction into the first orders can occur when $\Delta nd = \lambda/2$. Regardless the input polarization, the diffraction efficiency of the 0^{th} order remains same, while the first diffraction orders are sensitive to the ellipticity angle (χ) of the input polarization as shown in Fig. 5(b). By checking the Stokes parameters for diffracted orders, we confirmed the first orders have orthogonal circular polarization while the zeroth order has the same polarization state as the input. For all aspects of Eq. 1 and 2, the FDTD results show excellent agreement with the analytical solutions.

We also test the optical performance of LCPGs for an off-axis input by varying the angle of incidence. Fig. 6(a) shows the calculated diffraction efficiencies for different incident angles (θ_{inc}) from 0 to 45° when $\Delta nd = \lambda/2$ and $\Lambda = 40\lambda$. The 0^{th} order appears as the incident angle increases even in the $\lambda/2$ retardation condition. It can be explained by the fact that the effective retardation can vary with the propagation direction inside of the grating. Still, most ($\sim 99.5\%$) energy stays in the three diffraction orders (the 0^{th} and $\pm 1^{st}$) even at a fairly high incident angle up to $\theta_{inc} = 45^\circ$. However, the polarization state of the first order becomes elliptical rather than perfectly circular when $\theta_{inc} > 30^\circ$ of incidence. Slightly larger degradation in polarization property of the -1^{st} order is observed than that of the $+1^{st}$ order. Still, the LCPG retains its unique diffraction properties when $\theta_{inc} < 30^\circ$.

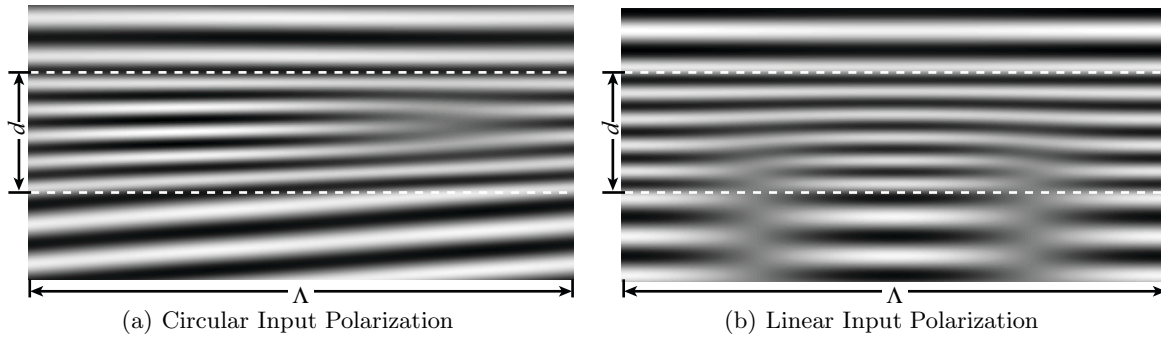


Figure 4. Near-field images of the electric field for (a) circularly polarized input and (b) linearly polarized input. The grating parameters are $\Lambda = 20\lambda$, $n_0 = 1.6$, $\Delta n = 0.2$, and $\Delta n d / \lambda = 0.5$.

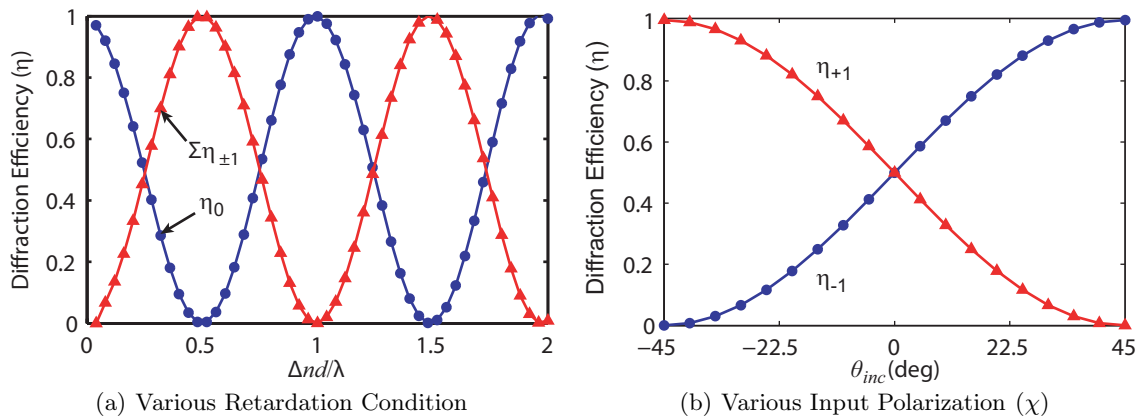


Figure 5. Diffraction efficiencies of the linear PG as a function of (a) the normalized retardation $\Delta n d / \lambda$ and (b) the ellipticity angle χ of the input polarization. The grating parameters are $\Lambda = 20\lambda_0$, $n_0 = 1.6$, and $\Delta n = 0.2$, where λ_0 is the center wavelength.

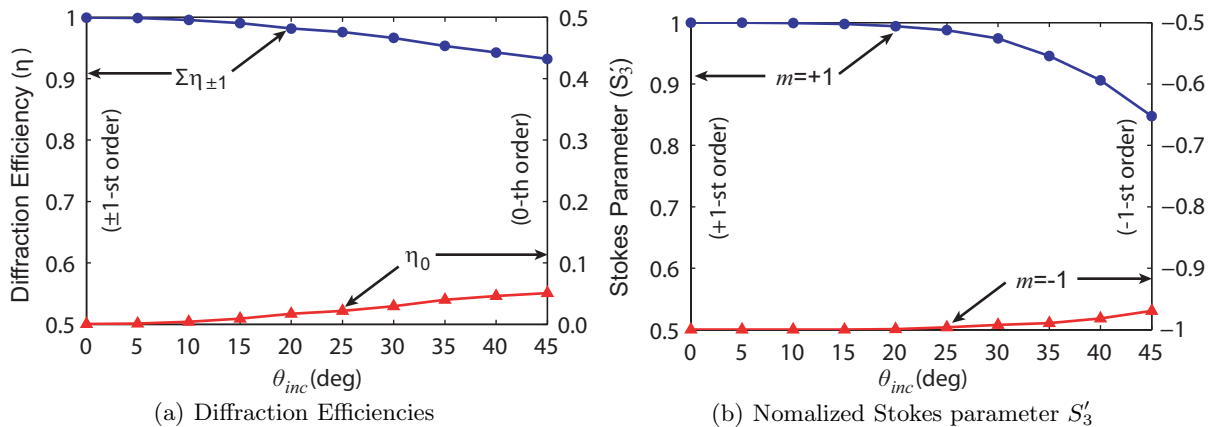


Figure 6. Diffraction properties of the LCPG at different incident angles (θ_{inc}): (a) diffraction efficiencies; (b) the normalized Stokes parameter $S'_3 (= S_3 / S_0)$ of the first orders. The incident light has a linear polarization.

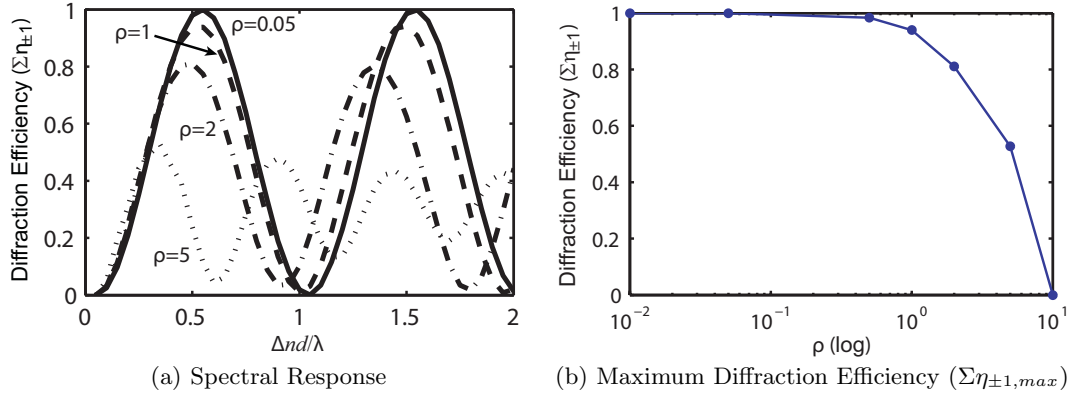


Figure 7. Diffraction properties of the LCPG for different values of the ρ parameter: (a) spectral response; (b) maximum achievable efficiency.

Light propagating in the LCPG diffracts in the paraxial limit, where thin gratings operate. The LCPG can be classified into the Raman-Nath (thin) grating regime even though it can perform a Bragg property; no higher diffraction order than the first orders. As mentioned earlier, the analytic expressions for the diffraction efficiencies of the LCPG were derived assuming paraxial approximations. One may expect that the unique diffraction properties of LCPGs will be degraded beyond the paraxial limit and the analytical solutions are no longer valid.

A traditional method to determine the grating regime is evaluating the grating parameters by a normalized parameter $Q = 2\pi\lambda d/\Lambda^2 n_0$ where n_0 is the average index of refraction of the medium.²⁴ Moharam²⁵ introduced an alternative method using the parameter $\rho = \lambda^2/\Lambda^2 n_0 n_1$ where n_1 is the index modulation factor. When the media has uniaxial birefringence, $n_0 \approx \frac{1}{2}(n_{\perp} + n_{\parallel})$ and n_1 can be replaced with $\Delta n/2$. For conventional gratings, the Raman-Nath behavior is expected when $Q < 1$ or $\rho < 1$ and the Bragg diffraction when $Q \gg 1$ or $\rho \gg 1$.

To test the paraxial limit of the LCPG, we varied grating parameters Λ and d for different values of Q and ρ . For FDTD optical simulations, only the grating thickness d was a variable for each ρ value and a monochromatic plane-wave was used instead of the Gaussian pulse. Also, we assumed that nematic directors retain the perfect sinusoidal LC configuration of Fig. 1(b) though the grating profile will be deformed when Λ is comparable to the thickness.¹⁵ Note that we directly used sine-functions for the nematic director profile, not from the LC3D calculations.

Fig. 7(a) shows the diffraction efficiency (a sum of $\eta_{\pm 1}$) for as a function of $\Delta nd/\lambda$. We found that the effect of ρ parameter dominates in the most cases of our interest. Especially, a significant degradation of the maximum diffraction efficiency was found for large ρ parameters as shown in Fig. 7(b). We note that the traditional threshold values for the gratings regimes may be still applicable to the LCPG; the thin (Raman-Nath) regime when $\rho \leq 1$; the Bragg grating regime when $\rho \gg 1$.

Electro-optic tuning or switching of the LCPG is possible by applying electric fields across the cell. Nematic directors in LCPGs are aligned according to the surface condition and they stay in the grating plane without applied fields. When an external field exceeding the threshold value is applied to the LCPG cell, the LC directors start to be reoriented along to the direction of the field as shown in Fig. 8(a).

To evaluate the effect of external fields, we vary the applied voltage (V_A) across the LCPG cell. The LC director angles, calculated from the LC3D configurations, are used to define grating structures at each applied voltage V_A . Fig. 8(b) shows the spectral response of the zeroth order transmission for different values of V_A . As mentioned earlier, the applied electric field leads in reorientation of LC directors resulting a red-shift of the diffraction spectrum because light propagating in the LCPG sees reduced effective retardation.

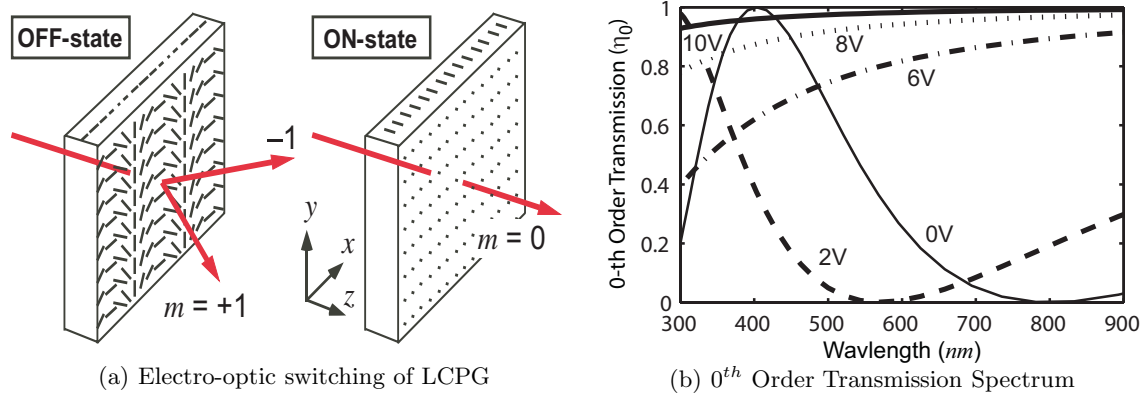


Figure 8. Electro-optic switching of the LCPG: (a) “ON” and “OFF” state of the LCPG; (b) spectral response of the 0th order transmission for different values of V_A .

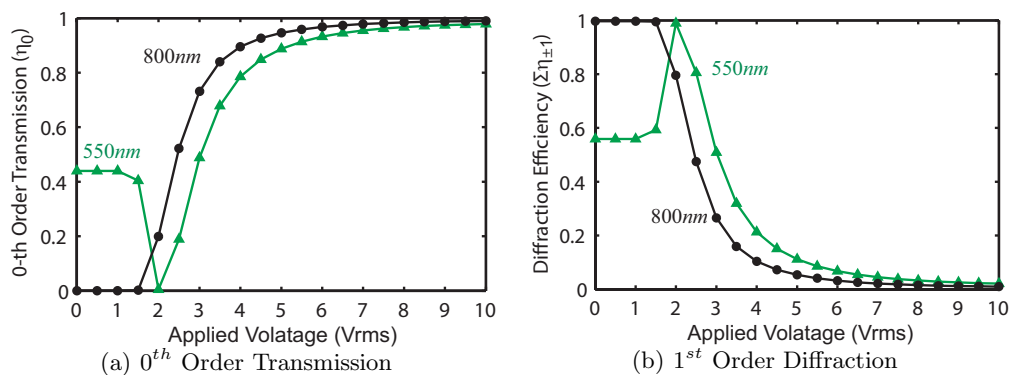


Figure 9. Diffraction efficiencies of the LCPG for various applied voltage (V_A): (a) the 0th order; (b) the first orders. The grating thickness is $2\mu\text{m}$ and the maximum diffraction occurs at 800nm , where $\Delta nd = \lambda/2$.

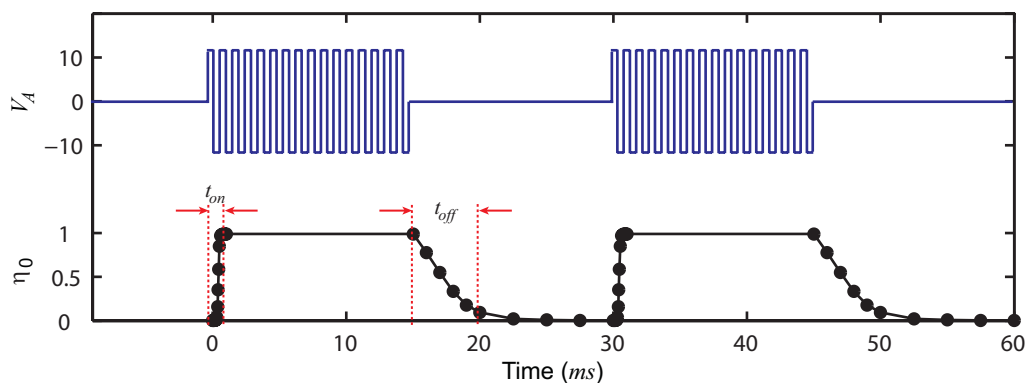


Figure 10. Dynamic response of the 0th order transmission at $V_A = 10\text{Vrms}$.

Basic switching behavior is illustrated in Fig. 9(a) and 9(b). The diffraction efficiencies (a sum of $\eta_{\pm 1}$) for two wavelengths, 550nm and 800nm, were calculated as a function of V_A . As expected in Ref. 14, the threshold voltage (V_{th}) is found around 1.5V. When $V_A > V_{th}$, the diffraction energy moves from the first orders to the 0th order as an applied voltage increases. Though the grating thickness is optimized for the maximum diffraction efficiency at 800nm, a high efficiency at other wavelengths can be achieved at $\sim 2V$.

Fig. 10 shows the dynamic response of LCPGs to a 10Vrms square wave. For all wavelengths, 0.6ms of rise-time (t_{on}) and 10ms of fall-time (t_{off}) are found. While the order of magnitude is similar, we note that the predicted switching times are longer than the previous experimental data ($t_{on} \simeq 0.2ms$ and $t_{off} \simeq 1.6ms$).¹⁴ Also, a time-delay ($\sim 0.2ms$) exists when “ON”-switching, which is not found for our LCPG samples. The discrepancy between numerical and experimental results shows that some of important dynamic aspects are missing in the LC director configuration calculations.

4. CONCLUSIONS

We have studied the optical properties of the LCPG diffraction using the FDTD method combined with LC3D. The angle information of nematic directors from LC configuration calculation results was used in optical analysis by the FDTD method. Basic diffraction characteristics of the LCPG have been successfully confirmed by the FDTD simulation results. The optical response of the LCPG to the off-axis input was tested. It was found that high diffraction efficiency can be achieved at a relatively high incident angle (i.e. 30°) with same diffraction properties; three diffraction orders (0th and $\pm 1^{st}$) and circularly polarized first orders. The electro-optic response of the LCPG was also tested for both static and dynamic situations. Electrical tuning and switching was observed in the FDTD optical simulations when $V_A > V_{th}$. Computer simulation results show good agreement with analytical solutions or previous experimental data. We believe that numerical methods (a combination of FDTD and LC3D) be very useful to optimize the LCPG design for more advanced performances.

ACKNOWLEDGMENTS

The authors gratefully acknowledge the support of the National Science Foundation through a STTR Phase I grant (OII0539552), in partnership with Southeast TechInventures Inc. and ImagineOptix Corp.

REFERENCES

1. P. J. Bos, J. Chen, J. W. Doane, B. Smith, C. Holton, and W. Glenn, “An optically active diffractive device for a high-efficiency light valve,” *J. Info. Display* **3**, pp. 195–197, 1995.
2. J. Chen, P. J. Bos, H. Vithana, and D. L. Johnson, “An electro-optically controlled liquid crystal diffraction grating,” *Appl. Phys. Lett.* **67**, pp. 2588–2590, 1995.
3. C. M. Titus and P. J. Bos, “Efficient, polarization-independent, reflective liquid crystal phase grating,” *Appl. Phys. Lett.* **71**, pp. 2239–2241, 1997.
4. B. Wang, X. Wang, and P. J. Bos, “Finite-difference time-domain calculations of a liquid-crystal-based switchable bragg grating,” *J. Opt. Soc. Am. A* **21**, pp. 1066–1072, 2004.
5. S. D. Kakichashvili, “Method of recording phase polarization holograms,” *Sov. J. Quant. Electron.* **4**, pp. 795–798, 1974.
6. L. Nikolova and T. Todorov, “Diffraction efficiency and selectivity of polarization holographic recording,” *Opt. Acta* **31**, pp. 579–588, 1984.
7. J. Tervo and J. Turunen, “Paraxial-domain diffractive elements with 100% efficiency based on polarization gratings,” *Opt. Lett.* **25**, pp. 785–786, 2000.
8. M. Ivanov and T. Eiju, “Analysis of the properties of polarization holographic diffraction gratings,” *Proc. SPIE* **4659**, pp. 361–368, 2002.
9. G. Cipparrone, A. Mazzulla, and L. Blinov, “Permanent polarization gratings in photosensitive langmuir-blodgett films for polarimetric applications,” *J. Opt. Soc. Am. B* **19**, pp. 1157–1161, 2002.
10. L. Nikolova, T. Todorov, M. Ivanov, F. Andruzzi, S. Hvilsted, and P. S. Ramanujam, “Polarization holographic gratings in side-chain azobenzene polyesters with linear and circular photoanisotropy,” *Appl. Opt.* **35**, pp. 3835–3840, 1996.

11. H. Sarkissian, B. Park, N. Tabirian, and B. Zeldovich, "Periodically aligned liquid crystal: potential application for projection displays and stability of lc configuration," *Optics in the Southeast 2003 conference program*, p. PSE 02.
12. J. N. Eakin, Y. Xie, R. A. Pelcovits, M. D. Radcliffe, and G. P. Crawford, "Patterned alignment layers using holographic exposure technique," *SID Digest* **04**, pp. 578–581, 2004.
13. J. N. Eakin, Y. Xie, R. A. Pelcovits, M. D. Radcliffe, and G. P. Crawford, "Zero voltage freedericksz transition in periodically alligned liquid crystals," *Appl. Phys. Lett.* **85**, pp. 1671–1673, 2004.
14. M. J. Escuti and W. M. Jones, "Polarization independent switching with high contrast from a liquid crystal polarization grating," *SID Digest* **37**, pp. 1443–1446, 2006.
15. C. Oh, R. Komanduri, and M. J. Escuti, "FDTD and elastic continuum analysis of the liquid crystal polarization grating," *SID Digest* **37**, pp. 844–847, 2006.
16. H. Sarkissian, N. Tabirian, B. Park, and B. Zeldovich, "Potential application of periodically aligned liquid crystal cell for projection displays," *Proc. of CLEO/QELS* **3**, pp. 1597–1599, 2005.
17. J. E. Anderson, P. E. Watson, and P. J. Bos, *LC3D: Liquid Crystal Display 3-D Director Simulation Software and Technology Guide*, Artech House Publishers, Boston, 2001.
18. Personal communication, manufacturer technical data sheet from Merk, 2005.
19. K. S. Yee, "Numerical solution of initial boundary value problems involving maxwell's equations in isotropic media," *IEEE Trans. Antenn. Propag.* **14**, pp. 302–307, 1966.
20. J. A. Roden, S. D. Gedney, M. P. Kesler, J. G. Maloney, and P. H. Harms, "Time-domain analysis of periodic structures at oblique incidence: Orthogonal and nonorthogonal fdtd implementation," *IEEE Trans. Microwave Theory Tech.* **46**, pp. 420–427, 1998.
21. C. Oh, "Finite-difference time-domain analysis of periodic anisotropic media," Master's thesis, North Carolina State University, Raleigh, NC, 2005.
22. S. D. Gedney, "An anisotropic perfectly matched layer-absorbing medium for the truncation of fdtd lattices," *IEEE Trans. Antenn. Propag.* **44**, pp. 1630–1639, 1996.
23. W. H. Southwell, "Gradient-index antireflection coatings," *Opt. Lett.* **8**, pp. 584–586, 1983.
24. H. Kogelink, "Coupled wave theory for thick hologram gratings," *Bell Syst. tech. J.* **48**, pp. 2909–2947, 1969.
25. M. G. Moharam and L. Yong, "Criterion for bragg and raman-nath diffraction regimes," *Appl. Opt.* **17**, pp. 1757–1759, 1978.